MSC INTERNAL NOTE NO. 67-EG-37

PROJECT APOLLO

CONTROLLABILITY DURING DPS THRUSTING

Prepared by: Henry J. G. Kaupp, Jr.

Approved: Kenneth J. Cox, Chief
Systems Analysis Branch

Approved: R. G. Chilton, Deputy Chief
Guidance and Control Division

RECEIVED
NASA STI FACILITY
INPUT BRANCH
AUG 1970

NATIONAL AERONAUTICS AND SPACE ADMINISTRATION

MANNED SPACECRAFT CENTER

HOUSTON, TEXAS

December 7, 1967

N70-34706

(ACCESSION NUMBER) (THRU)

14 1

(PAGES) (CODE)

TMX-64394 21

(NASA CR OR TMX OR AD NUMBER) (CATEGORY)

FACILITY FORM 602

Reproduced by
NATIONAL TECHNICAL INFORMATION SERVICE
Springfield, Va. 22151

Introduction

In case of a failure in the gimbal trim system (GTS) of the LM descent propulsion system (DPS), or an erroneous GTS drive command from the LM digital autopilot (DAP) caused by noisy attitude measurements, or large initial LM c.g. uncertainty due to propellant transfer during coast, it is possible for the disturbance torque due to DPS thrust to exceed the control torque available from the reaction jet control system (RCS). Attempts to plot controllability boundaries are generally complicated by the fact that there are numerous time varying parameters, and that pitch and roll RCS torques are coupled. This note discusses the LM controllability problem in a general sense, and presents a nomogram that should be a useful tool for quick assessments of stability margins (or divergence rates) for specific cases.

Disturbance Moments

Figure 1 shows the LM coordinate system. Also shown are the unit vectors $\bar{i}$, $\bar{j}$, $\bar{k}$, which are defined to be in the $+X_B$, $+Y_B$, $+Z_B$ axis directions, respectively. The disturbance moment in the control axes is developed below with the aid of figure 2.

Define: (a) $\ell = X_{cg} - X_g$, where X_{cg} is the location of the c.g. along the X_B axis and X_g is the location of the DPS gimbal.

(b) δ_Y, δ_Z - the thrust orientation angles defined as rotations in the positive sense about Y and Z body axes, respectively.

From the geometry of figure 2, and assuming small angles for δ_Y and δ_Z, the following can be written:

$$\bar{P} \cong [\delta_Z \bar{j} - \delta_Y \bar{k}]\ell \tag{1}$$

$$\bar{C} = Y_{cg} \bar{j} + Z_{cg} \bar{k} \tag{2}$$

$$\bar{L} = \bar{C} - \bar{P} \tag{3}$$

$$\bar{T} = T \bar{i} + T \delta_Z \bar{j} - T \delta_Y \bar{k} \tag{4}$$

The physical interpretations of these vectors are as follows. $\bar{P}$, $\bar{C}$, and $\bar{L}$ all lie in the $Y_B Z_B$ plane. $\bar{P}$ is a two component vector of the coordinates for the thrust vector intersection with this plane and $\bar{C}$ is a two component vector of the coordinates for the center of mass location in this plane. The difference of these vectors ($\bar{L}$) is the straight line distance from the thrust intersection to the c.g. position and also contains direction information for determination of the disturbance torque.

The disturbance torque ($\bar{M}_{DPS}$) is the vector cross product $\bar{T} \times \bar{L}$.

$$\bar{M}_{DPS} = \bar{T} \times \bar{L} = \begin{vmatrix} \bar{i} & \bar{j} & \bar{k} \\ T & T\delta_Z & -T\delta_Y \\ 0 & (Y_{cg} - \ell\delta_Z) & (Z_{cg} + \ell\delta_Y) \end{vmatrix} \tag{5}$$

$$\bar{M}_{DPS} = T[\delta_Z Z_{cg} + \delta_Y Y_{cg}]\,\bar{i} - T\,[Z_{cg} + \ell\delta_Y]\,\bar{j} + T\,[Y_{cg} - \ell\delta_Z]\,\bar{k} \tag{6}$$

Controllability

It should be noted that the first term of equation (6) is second order and no problem with controllability will be encountered in yaw (rotations about X); therefore, the remainder of this document will deal only with controllability in pitch and roll (rotations about Y and Z, respectively). For stable operation, either one of two events must occur. Either the GTS must act to drive $\bar{L}$ to zero (pass the DPS thrust through the center of mass), or $\bar{L}$ must be smaller than the available RCS torque expressed in terms of how much disturbance lever arm it will compensate.

$$|\bar{L}| \leq |\bar{L}_{RCS}| \tag{7}$$

In the event that equation (7) is not satisfied the vehicle is unstable and the angular acceleration is given by

$$\dot{\bar{\omega}} = \frac{\bar{T}}{I} \times (\bar{L} - \bar{L}_{RCS}) \tag{8}$$

Due to the geometry of jet thruster location on the LM vehicle, available RCS torque is a function of the relative amounts of pitch and roll components. Maximum torque is available for pure pitch or pure roll, but combinations result in reduced maximum capability due to creation of conflicting requirements for linear forces at specific thruster quads.

The available RCS torque limit, as a function of torque direction in the c.g. plane, is plotted in figure 3 for two options of jet select logic (two or four jet couples). Superimposed on this plot is an example of DPS mistrim and RCS torque vectors for the limit controllability condition.

The objective is to determine limit magnitudes of the mistrim distance, $\bar{L}_{RCS}(\bar{C}, \bar{T}, \ell)$, using maximum available RCS torque as the constraint. Toward this end the mistrim torque is equated to the negative of the limit magnitude of RCS torque, the limit condition for controllability.

$$\bar{M}_{RCS} = -\bar{M}_{DPS} = -\bar{T} \times \bar{L}_{RCS} \tag{9}$$

If the vector $\bar{T}$ is crossed into both sides of equation (9)

$$\bar{T} \times \bar{M}_{RCS} = \bar{T} \times (-\bar{T} \times \bar{L}_{RCS}) \tag{10}$$

$$= -\bar{T}(\bar{T} \cdot \bar{L}_{RCS}) + \bar{L}_{RCS}(\bar{T} \cdot \bar{T})$$

Recalling that the dot products are scalars, and that $\bar{T}$ is nearly perpendicular to $\bar{L}$ (maximum deviation from perpendicular is six degrees), we have the final result

$$\bar{L}_{RCS} \approx 1_{\bar{T}} \times \frac{\bar{M}_{RCS}}{|T|} \tag{11}$$

Equation (11) shows that a plot of limit values for $\bar{L}(\bar{L}_{max} = (\bar{L}_{RCS})_{max})$ can be constructed from the plot of limit values for $\bar{M}_{RCS}$ shown in figure 3. This is done by scaling each point on figure 3 by the factor 1/T and rotating the point 90 degrees CCW. The resulting plot appears as figure 4.

Nomograms for LM Descent Controllability

This section presents the results of an analysis of LM control authority in such a manner that controllability margin can be determined for any desirable combination of the four parameters, flight time, DPS thrust magnitude, pitch mistrim, and roll mistrim. First, the boundaries of all possible thrust intersections with the c.g. plane ($\bar{P}$) (due to the mechanical limits of the gimbal) are plotted for four separate times of flight in figure 5. RCS control limit boundaries for $\bar{L}$ appear in figure 6 for four combinations of RCS moments and DPS thrust levels. Placing the origin of figure 6 on the point of DPS thrust intersection on figure 5, with the axes parallel, shows the allowable limits of c.g. location for a controllable system. Alternately, the maximum c.g. "capture" capability in any given direction assuming perfect operation of the GTS is obtained by moving the origin of figure 6 to the $\bar{P}$ boundary in that direction and determining the amount of additional range allowable without exceeding the limit value of $\bar{L}$.

It should be noted that the question of whether or not the vehicle is controllable can be thought of as a function of seven variables, each of which is a function of time. This can be expressed as:

$$\text{CONTROLLABILITY} = f(X_{cg}, Y_{cg}, Z_{cg}, |T|, \delta_Y, \delta_Z, \text{JETNO})$$

where JETNO is the number of RCS jets available. The analysis approach documented in this note breaks the complex function down into three more tractable functions.

$$\overline{P} = f_1 (X_{cg}, \delta_Y, \delta_Z)$$

$$\overline{C} = f_2 (Y_{cg}, Z_{cg})$$

$$\overline{L}_{RCS} = f_3 (\text{JETNO}, |T|, \delta_Y, \delta_Z)$$

and presents the relationship between the component functions in graphical form. The following section presents a specific example of how the graphical aids are used.

Shown in figure 7 is the maximum range of change in c.g. for shifts in the propellant from one tank to another. Figure 8 shows the arrangement of the LM tanks. It can be noted that a shift in the oxidizer has little effect on the Y c.g. since the tanks are located symmetrically on the control axes, and, likewise, a shift in the fuel has little effect on the Z c.g. Thus, figures 5, 6, and 7 can be used in determining controllability with OFF-nominal propellant loading conditions.

Example Problem

In order to show the use of figures 5 and 6, consider the following problem: The descent engine is hardover near touchdown, in the δ_Y direction. Is the LM stable, and if not, can an abort stage be accomplished if the main engine remains at full thrust (10,500 lbs) for two seconds before staging? Whether or not the abort stage can be accomplished is dependent on the rotation rates of the spacecraft at the beginning of the sequence (present constraints suggest anything above 3°/sec is prohibitive). Looking at figure 5, it can be seen that at touchdown the descent engine thrust vector crosses the c.g. plane at $Y_B = 0.0$, $Z_B = -0.55$ ft. (This point denoted by ⊙ on figure 5.) The nominal c.g. is located at $Y_B = +0.03$, $Z_B = +0.028$ ft (denoted by "X" in figure 5). This situation gives a disturbing moment of -6,080 ft-lb in pitch and +315 ft-lb in roll. By superimposing figure 6 on the thrust vector it can be seen that the RCS cannot compensate for the mistrim of the engine; therefore, the vehicle is uncontrollable. Assuming four jet operation and

full descent engine thrust, curve (b) the effective moment arm is determined as shown by the example construction on figure 5. Here we see that the net moment arm is roughly 0.4 ft. It can be noted that if the main engine thrust is reduced to somewhere between 5,250 and 2,625 lbs the spacecraft is stable. The exact thrust required for controllability could be found by interpolation between these values. If the unbalanced moment remained at 4,200 ft-lb for two seconds, the rate attained in pitch would be in excess of 30°/seconds, which is completely unacceptable for abort staging.

Conclusion

This note has presented the results of an analysis which allows rapid determination of static stability and moments on the LM spacecraft due to descent engine mistrim.

These same results apply for ascent problems, where the situation is simpler because ascent engine is fixed, and thus the thrust intersection would be a series of points in figure 5. In addition, only two boundaries would appear on figure 6 because the ascent engine has only one possible value of thrust. Results for ascent have already been documented by GAEC.

Some error is introduced in using these figures due to the small angle approximations made in obtaining the descent engine arm. The largest possible error, however, is 4.5 percent, and this would represent an extreme case. The error is also conservative since the computed mistrim torque is larger than the real torque.

Some comment should be made about the yaw moments due to a mistrim of the descent engine. Equation 6 shows that if the descent engine is not in trim, a yaw moment is also generated. This component of mistrim torque should never exceed the yaw RCS torque capability. Although it is expected that this disturbance will be small on the average, if it should persist for extended periods of time, the RCS propellant usage for yaw (X-axis) attitude control could be increased significantly.

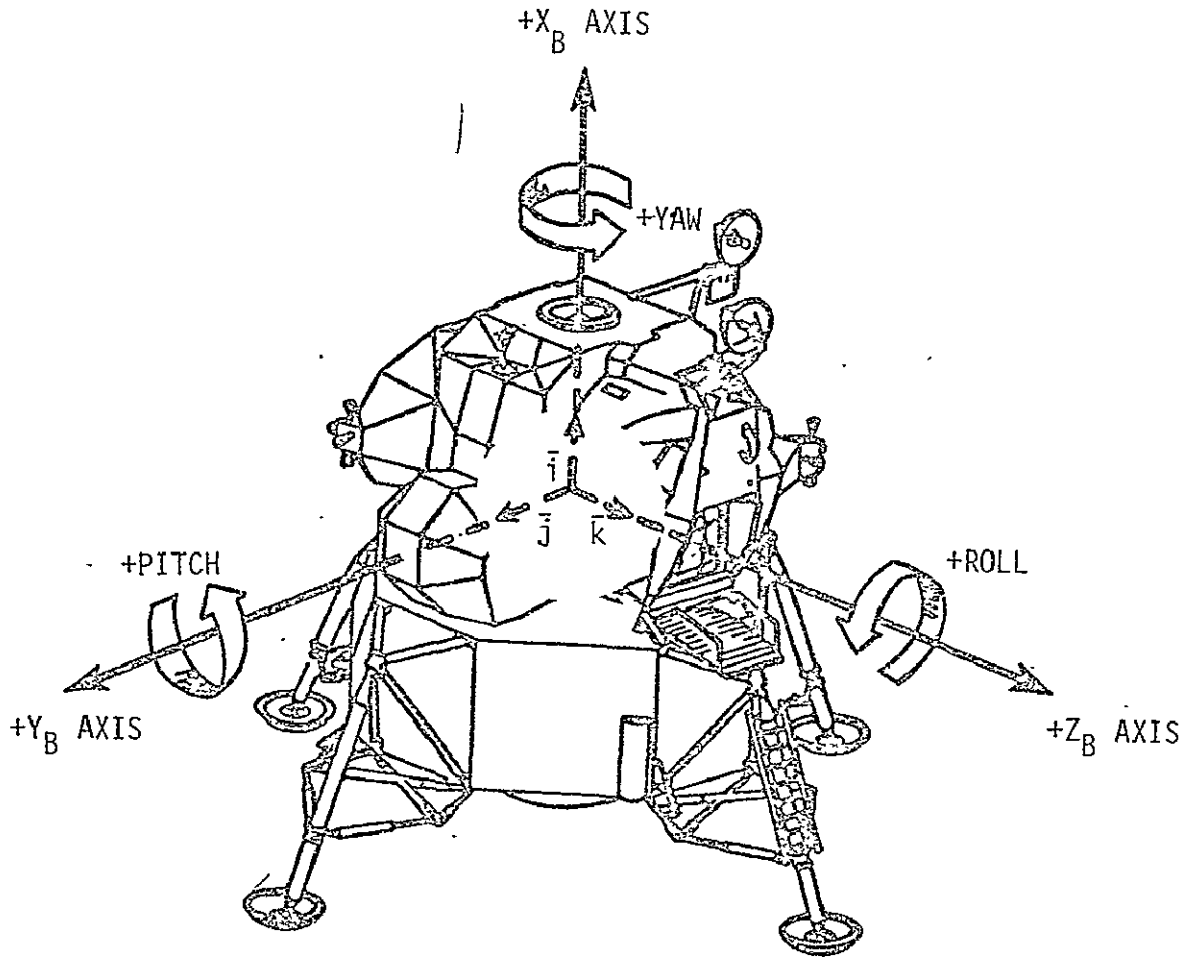

LM VEHICLE AXIS

X_B AXIS: LM Vehicle Yaw Axis

Y_B AXIS: LM Vehicle Pitch Axis

Z_B AXIS: LM Vehicle Roll Axis

Note: The XZ - plane contains the mass center and the X_B axis is the longitudinal axis of symmetry.

Figure 1.- LM Coordinate System

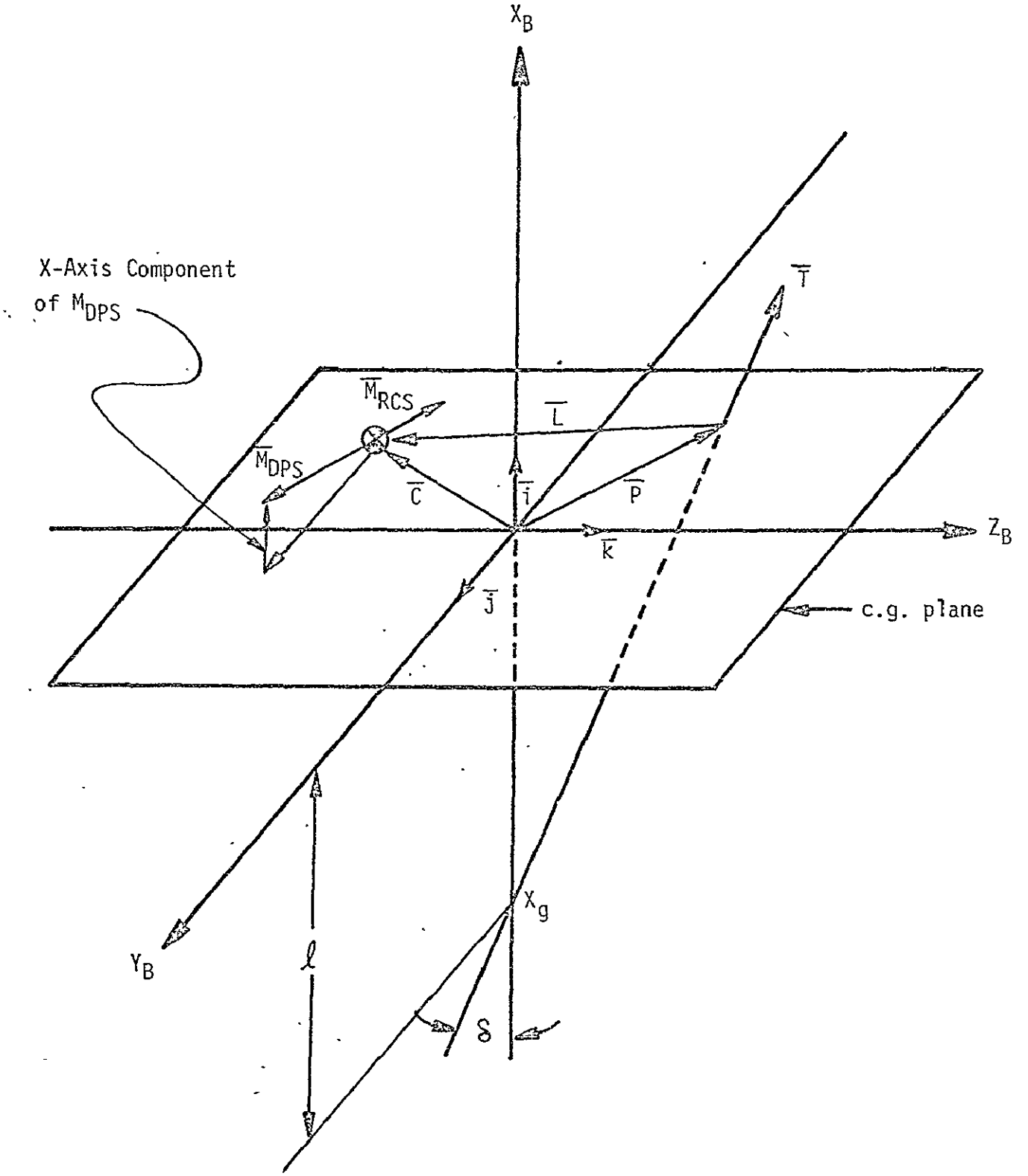

Figure 2.- Geometry of Disturbance Moment

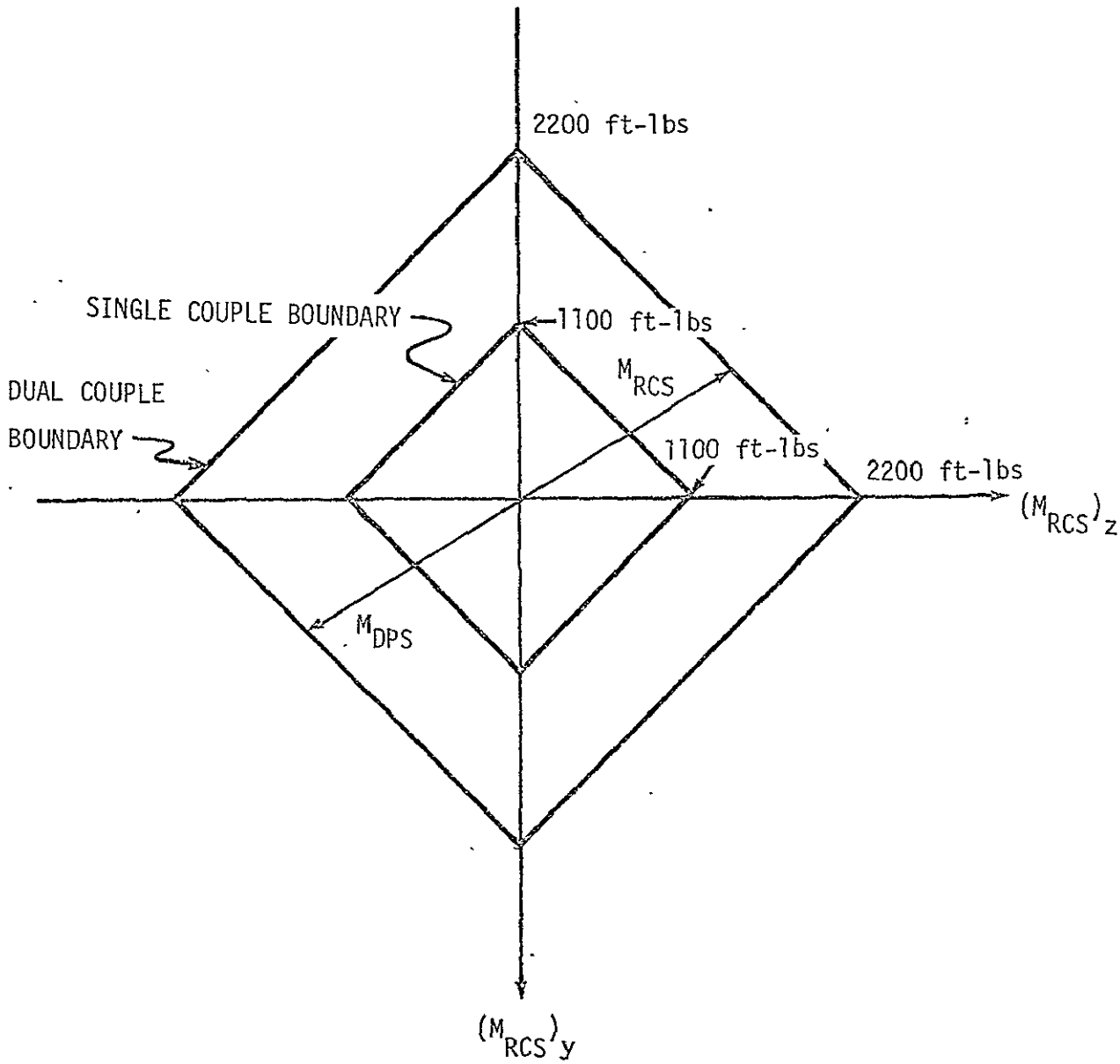

Figure 3.- LM RCS Torque Limit Boundaries (PGNCS DAP Only)

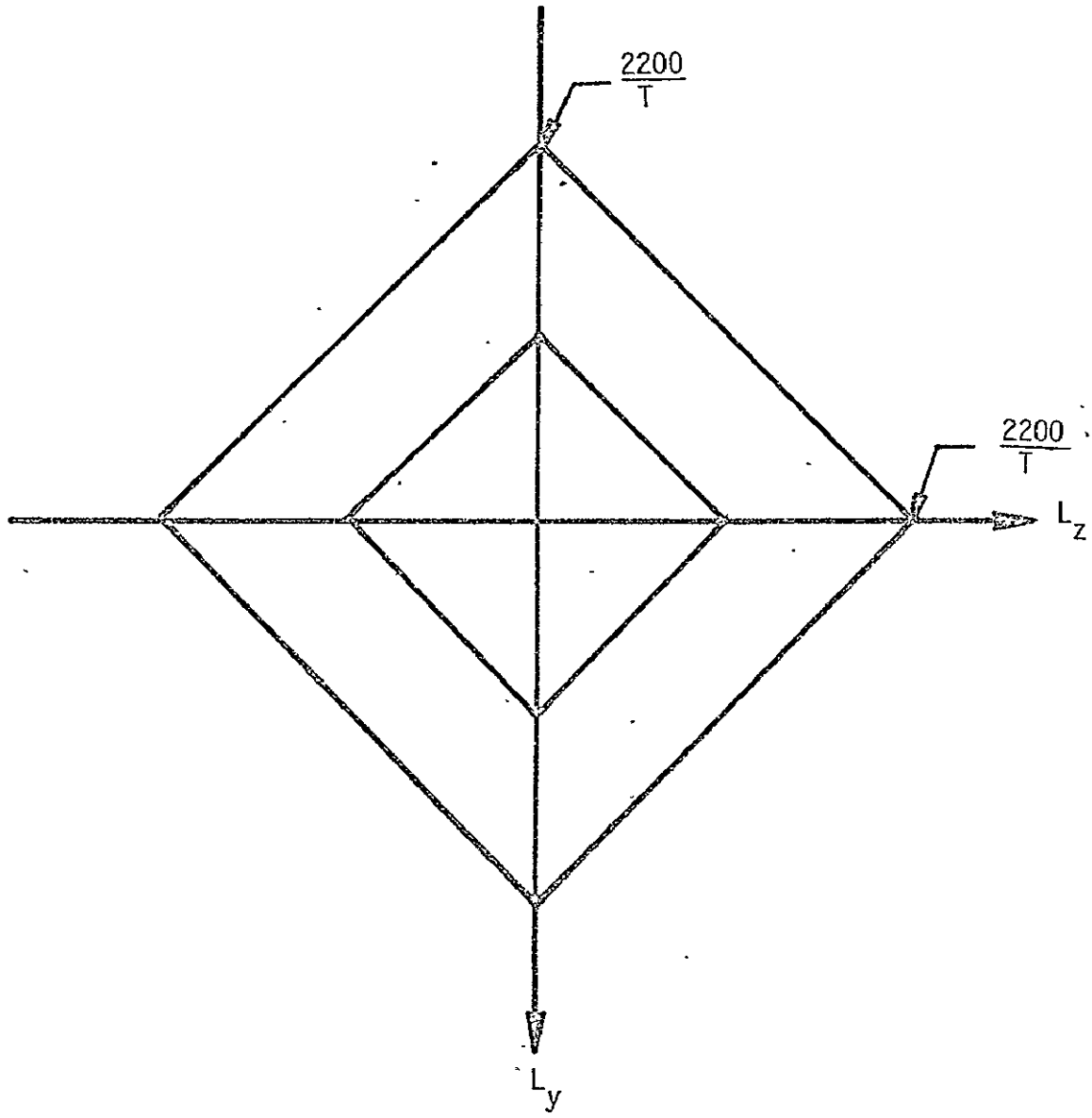

Figure 4.- Limit Values of $\vec{L}$

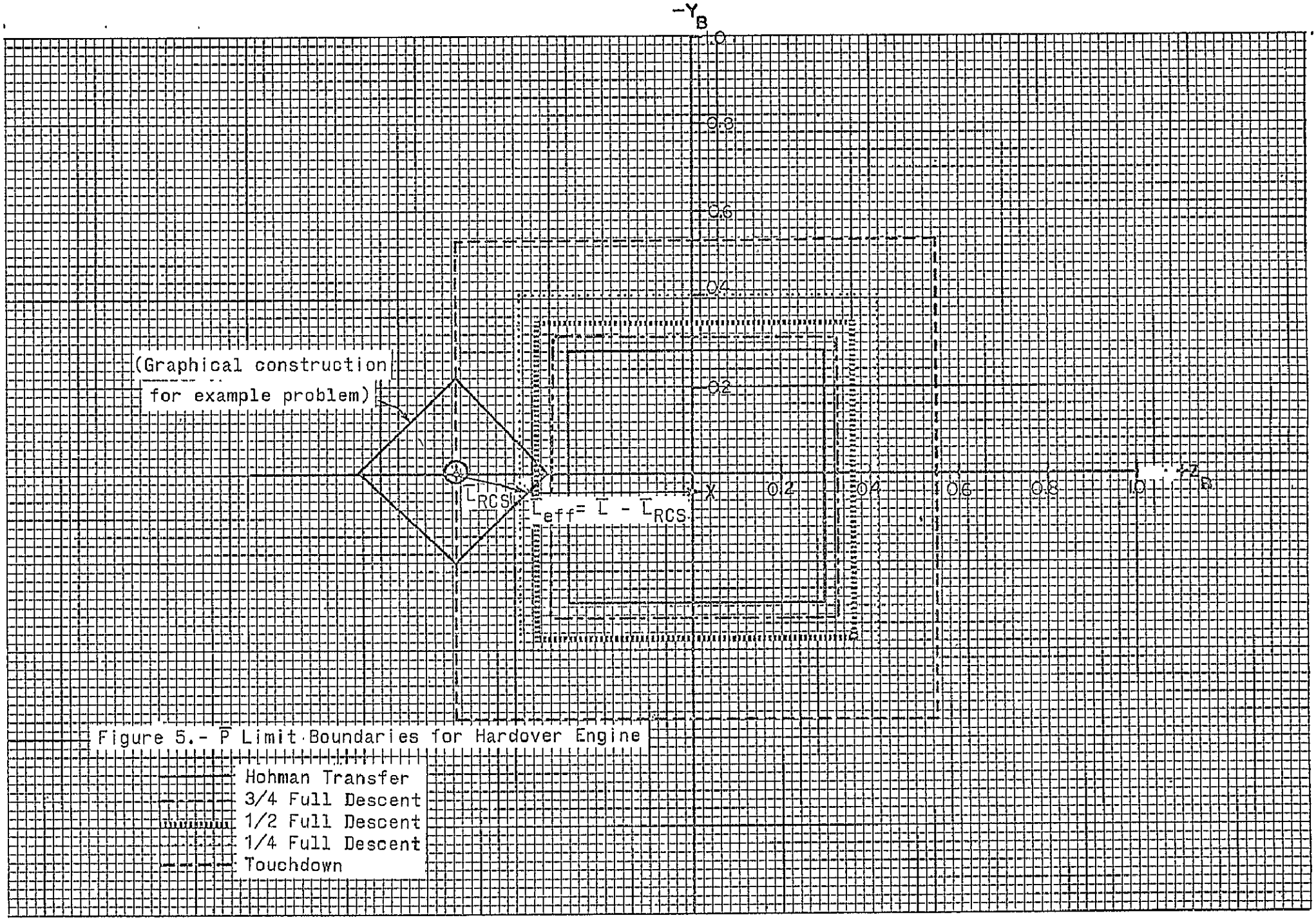

Figure 5.- $\bar{P}$ Limit Boundaries for Hardover Engine

LEGEND

A 1100 ft-lb with 10,500 lb Thrust
B 2200 ft-lb with 10,500 lb Thrust; 1100 ft-lb with 5,250 lb Thrust
C 2200 ft-lb with 5,250 lb Thrust; 1100 ft-lb with 2,625 lb Thrust
D 2200 ft-lb with 2,625 lb Thrust; 1100 ft-lb with 1,312 lb Thrust

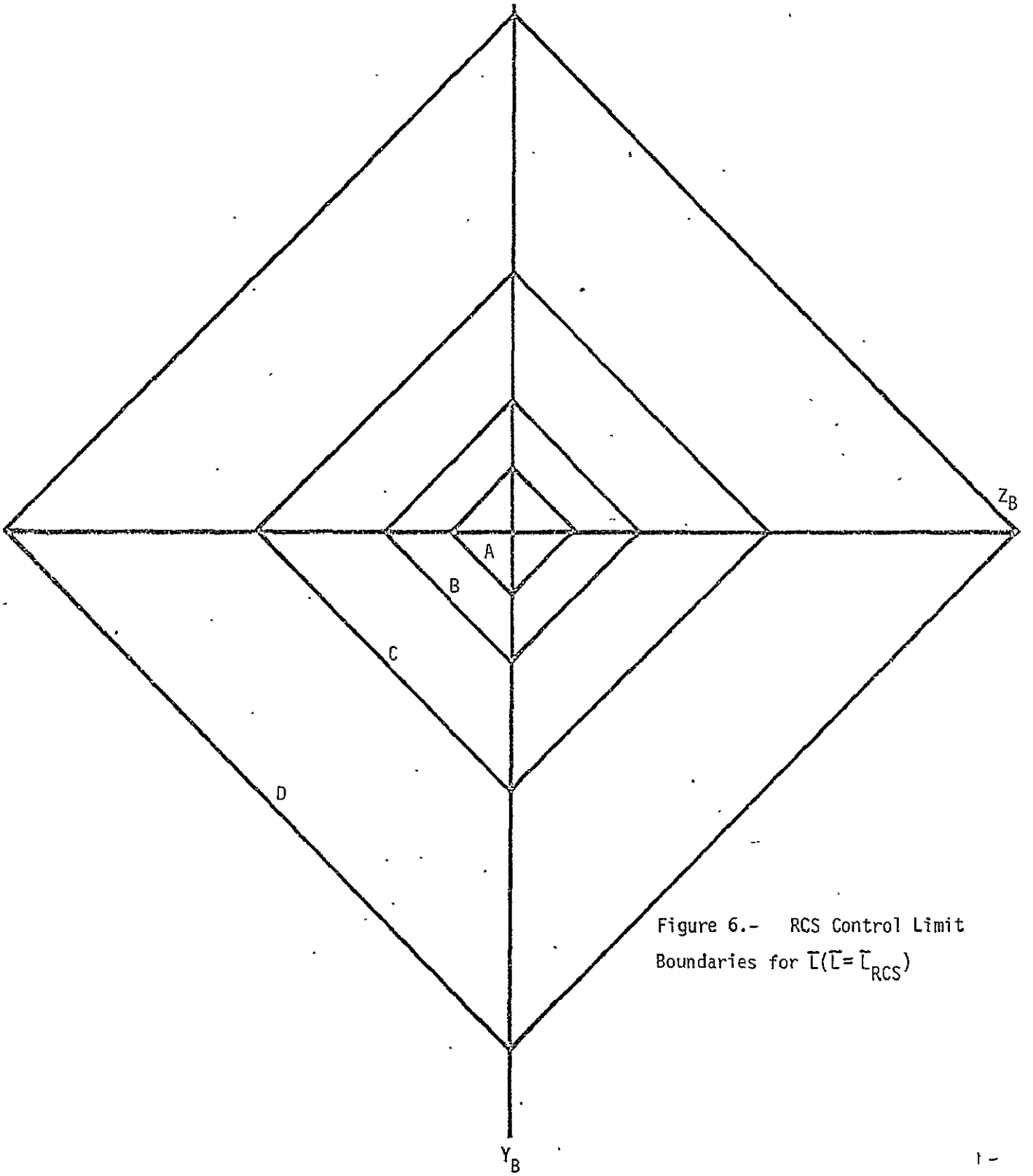

Figure 6.- RCS Control Limit Boundaries for $\bar{L}(\bar{L} = \bar{L}_{RCS})$

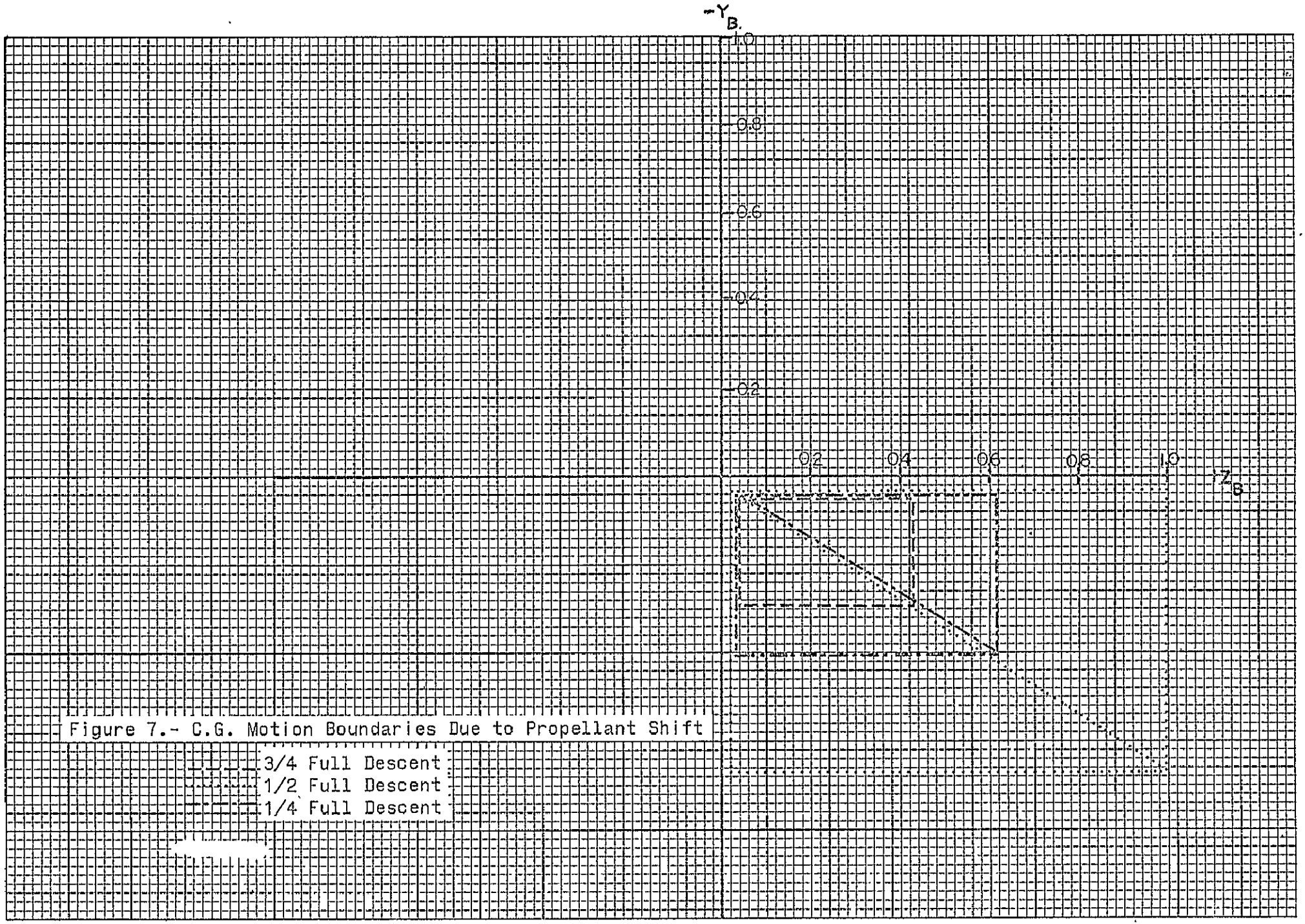

Figure 7.- C.G. Motion Boundaries Due to Propellant Shift

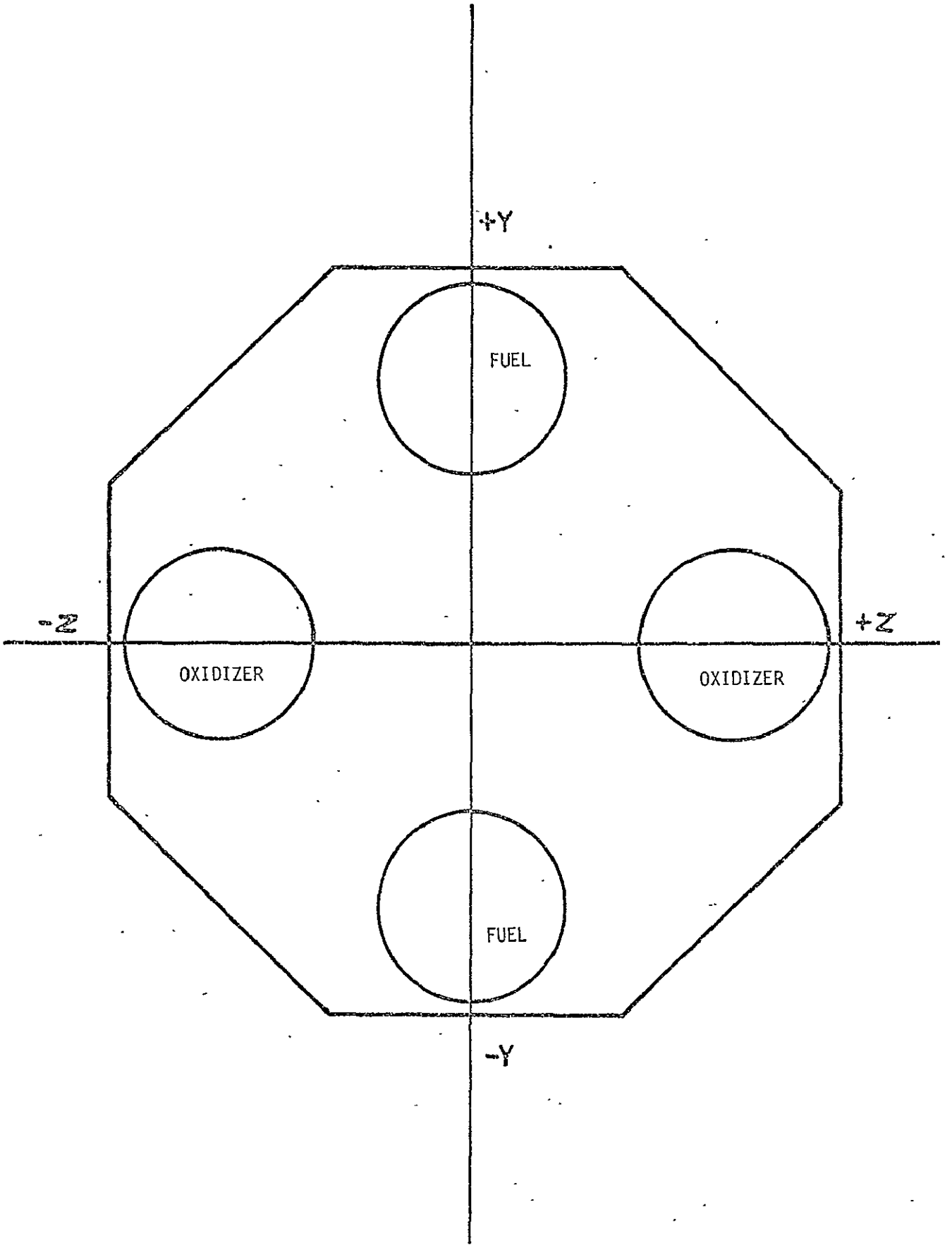

Figure 8.- LM Tank Positions (Descent)